Study of the ^{4}He(^{4}He,^{4}He)^{4}He* inelastic scattering at the MAGNEX facility

V. Soukeras[1,2*], *F.* Cappuzzello[1,2], *M.* Cavallaro[1], *D.* Carbone[1], *A.* Hacisalihoglu[1,3], *M.* Fisichella[1], *C.* Agodi[1], *H.-W.* Becker[4], *G. A.* Brischetto[1,2], *S.* Calabrese[1,2], *C.* Ciampi[5], *M.* Cicerchia[6], *M.* Cinausero[6], *I.* Ciraldo[1,2], *M.* D´ Andrea[7], *D.* Dell´ Aquila[8], *S.* Firat[9], *C.* Frosin[5], *M.* Hilcker[4], *L.* La Fauci[1,2], *I.* Lombardo[7], *T.* Marchi[6], *O.* Sgouros[1], *A.* Spatafora[1,2], *D.* Torresi[1], *M.* Vigilante[10], and *A.* Yildirim[9]

[1]INFN – Laboratori Nazionali del Sud, Catania, Italy
[2]Dipartimento di Fisica e Astronomia "Ettore Majorana", Università di Catania, Catania, Italy
[3]Institute of Natural Science, Karadeniz Teknik Universitesi, Trabzon, Turkey
[4]Ruhr-Universitat Bochum, Bochum, Germany
[5]INFN – Sezione di Firenze, Florence, Italy
[6]INFN – Laboratori Nazionali di Legnaro, Legnaro, Italy
[7]INFN – Sezione di Catania, Catania, Italy
[8]Rudjer Bošković Institute, Zagreb, Croatia
[9]Akdeniz University, Antalya, Turkey
[10]INFN – Sezione di Napoli and Università degli Studi di Napoli "Federico II", Napoli, Italy

Abstract. The ^{4}He(^{4}He,^{4}He)^{4}He* inelastic scattering was revisited in a new coincidence measurement at the MAGNEX facility of Istituto Nazionale di Fisica Nucleare – Laboratori Nazionali del Sud. The ^{4}He + ^{4}He → ^{4}He + ^{4}He* → ^{4}He + ^{3}H + ^{1}H and ^{4}He + ^{4}He → ^{4}He + ^{4}He* → ^{4}He + ^{3}He + n reactions were measured simultaneously by detecting the ^{4}He particles at the MAGNEX magnetic spectrometer in coincidence with the ^{3}H and ^{3}He at the OSCAR silicon telescope. The main concept of the experiment is described and the data reduction strategy is reported.

1 Introduction

The ^{4}He is a well bound nucleus with a breakup threshold of 19.8 MeV for the ^{3}H – ^{1}H mode and 20.7 MeV for the ^{3}He – n one. No bound states are existing in its level scheme however it exhibits, very close to the breakup threshold, a pronounced resonance with the same spin and parity (0^+) as the ground state. Several investigations have been performed so far aiming at shedding light on the characteristics of this resonance either by using a ^{4}He(e,e´)^{4}He* [1-4] or a ^{4}He(^{4}He,^{4}He)^{4}He* [5-6] reaction.

Additionally, a recent ab-initio calculation of the monopole transition form factor of ^{4}He with realistic nuclear forces pointed to a strong dependence on the different realistic potential used and revealed a significant disagreement with respect to all existing electron scattering data when a method based on modern Hamiltonians from chiral perturbation theory was adopted [7]. The inconsistencies met between the recent ab-initio form factor and all existing data from ^{4}He(e,e´)^{4}He* studies call for further investigation.

In a recent theoretical work [8], the transition densities to the 0^+ excited state of ^{4}He were calculated and the form factors were constructed by folding procedure. The cross section angular distributions were also calculated for this state by using both macroscopic and microscopic models for the form factors.

From both the experimental and theoretical point of view the ^{4}He(e,e´)^{4}He* and ^{4}He(^{4}He,^{4}He)^{4}He* studies are challenging. The first ones give a direct access to the form factor, which is governed by a pure electromagnetic interaction. However, only the protons are involved in the interaction. Other disadvantages of (e,e´) include its very low cross section, the fact that it consists of a mixed isoscalar and isovector probes and finally, higher multipolarities are not possible to be excluded. On the other hand, the ^{4}He(^{4}He,^{4}He)^{4}He* studies benefit by a pure isoscalar probe, a significantly higher cross section and the higher multipolarities are easier to be unfolded. Nevertheless, the ^{4}He induced scattering is governed by the nuclear force, making the extraction of the electric monopole form factor less direct. In addition, an optical model analysis is needed to describe the distortions in the incoming and outcoming waves due to the initial and final state nucleus-nucleus interactions.

Taking into account the positive and negative features of the (^{4}He,^{4}He) probe, we performed inelastic scattering measurements for the ^{4}He + ^{4}He reaction at 53 MeV incident energy ($E_{c.m.}$ = 26.5 MeV) in order to extract the characteristics of the 0^+ resonance of ^{4}He in a new measurement and resolve previous

* Corresponding author: vasileios.soukeras@lns.infn.it

inconsistencies. Our study includes also a careful description of the significant phase space for both the ^{3}H – ^{1}H and ^{3}He – n modes. Finally, a global interpretation together with the elastic scattering channel, which was also measured, ensures a precise optical model analysis, allowing the extraction of the form factors.

2 The experiment

The ^{4}He beam was accelerated by the K800 Superconducting Cyclotron of Istituto Nazionale di Fisica Nucleare – Laboratori Nazionali del Sud (INFN – LNS) at 53 MeV and impinged on a ^{4}He target implanted on a thin aluminum foil. Measurements with a 2 MeV ^{4}He were performed at Ruhr – Universitat Bochum before the implantation in order to test the thickness and the uniformity of the aluminum foils while the ^{4}He scattering centres after the implantation were measured by a measurement with a 2.2 MeV proton beam at the same laboratory. The density of scattering centres of the ^{4}He as well as the other target materials, namely aluminum, oxygen and carbon are presented in Table 1. The measurement was repeated with a target composed of aluminum, oxygen and carbon in the appropriate proportions for the background estimation. However, the majority of the background events was excluded by performing the coincidence measurement described below.

Table 1. The density of scattering centres of helium, aluminum, oxygen, and carbon atoms present in the target.

Material	Thickness (at/cm^2)	Thickness (μg/cm^2)
He	1.92 E+17	1.29
Al	4.64 E+18	210
O	1.00 E+17	2.66
C	1.20 E+16	0.24

2.1 Elastic scattering measurement

The ^{4}He ejectiles were momentum analysed by the MAGNEX magnetic spectrometer [9] whose optical axis was set at θ_{opt} = 6.6° spanning an angular range between 2° and 13°. The different ions were detected by the Focal Plane Detector (FPD) [10-11] of MAGNEX, which consists of a gas tracker followed by a wall of 60 silicon pad detectors. The gas tracker includes six sections, each one having at the top a proportional wire. The energy loss (ΔE) of the ions inside the gas is measured in each of the six wires from the charge signal generated by the proportional multiplication of the primary electrons close to the wires. The residual energy (E_{resid}) is measured by the silicon pad detectors. The charge generated by the electron avalanches close to the multiplication wires is also induced into a segmented anode featuring a pattern of 223 independent pads. The anode is mounted above each DC wire allowing the measurement of the horizontal position (X_{foc}) and angle (θ_{foc}). The measurement of the electron drift time inside the gas allows the determination of the vertical position (Y_{foc}) and angle (φ_{foc}).

2.2 Inelastic scattering measurement

No bound states are reporting in ^{4}He structure [12] therefore the ^{4}He* excited states can be reconstructed by the detection of its fragments. In particular, the two different decay modes ^{4}He + ^{4}He → ^{4}He + ^{4}He* → ^{4}He + ^{3}H + ^{1}H and ^{4}He + ^{4}He → ^{4}He + ^{4}He* → ^{4}He + ^{3}He + n were reconstructed by two coincidence measurements. In both modes ^{4}He nuclei were detected by the MAGNEX FPD [11], while the ^{3}H and ^{3}He fragments were detected by OSCAR (hOdoscope of Silicons for Correlations and Analysis of Reactions) telescope [13]. OSCAR consists of two detection stages: a Single Sided Silicon Strip Detector (SSSSD) 20 μm thick as ΔE, followed by 16 silicon pads (4x4) 300 μm thick, providing the measurement of the residual energy E. OSCAR telescope was mounted inside the scattering chamber of MAGNEX, 15 cm from the target spanning the angular range between 19° and 38°. The 16 strips of the SSSSD allowed a measurement with an angular resolution of about 1°. The detection threshold in OSCAR was 2.5 MeV for ^{3}H, 5.0 MeV for ^{3}He and 5.5 MeV for ^{4}He, taking into account the SSSSD thickness and the electronics threshold for both ΔE and E.

3 Data Reduction

The particle identification (PID) of the data collected by the MAGNEX FPD was performed as described in Ref. [14]. The first step is the selection of the data belonging to the Z of interest ($Z = 2$) in a $\Delta E – E$ plot (Fig. 1). The mass separation is feasible by applying the appropriate graphical selection conditions to the $X_{foc} – E_{resid}$ spectra, where the different loci correspond to ions with different $\sqrt{m}/q$. Such a spectrum for a single silicon detector is illustrated in Fig. 2. Having identified the events of interest, a software 10th order ray – reconstruction [15] is applied to the data in order to obtain the kinetic energy, scattering angle, and excitation energy spectra.

The standard $\Delta E – E$ technique was applied for a precise PID at the OSCAR telescope and a typical $\Delta E – E$ plot is shown in Fig. 3.

The experimental inelastic scattering data collected by the two coincidence measurements were compared with kinematical simulations based on the multipurpose Monte Carlo simulation algorithm MULTIP [16]. This algorithm is a powerful tool for two –, three – and four – body reactions kinematics and its validity has been tested in several works and for many reactions [17-24]. In the present work, the inelastic scattering reaction ^{4}He + ^{4}He → ^{4}He + ^{4}He* → ^{4}He + ^{3}H + ^{1}H was simulated for both the resonant (0^{+}) and the non – resonant breakup, while the ^{4}He + ^{4}He → ^{4}He + ^{4}He* → ^{4}He + ^{3}He + n was simulated only for the non – resonant breakup since its threshold is higher than the 0^{+} resonant region. The transfer processes ^{4}He + ^{4}He → ^{3}H + ^{5}Li → ^{4}He + ^{3}H +

^{1}H and ^{4}He + ^{4}He → ^{3}He + ^{5}He → ^{4}He + ^{3}He + n leading to the same final channels were also simulated. The experimental data compared with the kinematical simulations are illustrated in Figs. 4 – 5 for the two different modes showing an excellent agreement themselves. It should be noted that except the importance at the preparation of the experiment, the simulations were also useful in order to estimate the energy efficiency due to the coincidence measurements. This efficiency is mainly dominated by the detection threshold of OSCAR, mentioned in section 2.2. The energy efficiency was extracted by taking the ratio between the simulated events with all the experimental conditions in angle, kinetic energy and excitation energy and the simulated events without the kinetic energy conditions. Since the efficiency may change for different excitation energy regions and angles, it was extracted for a step of dE_x = 0.8 MeV and $d\theta_{lab}$ = 0.5°, ensuring a precise estimation. Finally, the solid angle of both MAGNEX and OSCAR was deduced by geometrical simulations taking into account for the case of OSCAR the possible "dead regions" of its E – stage.

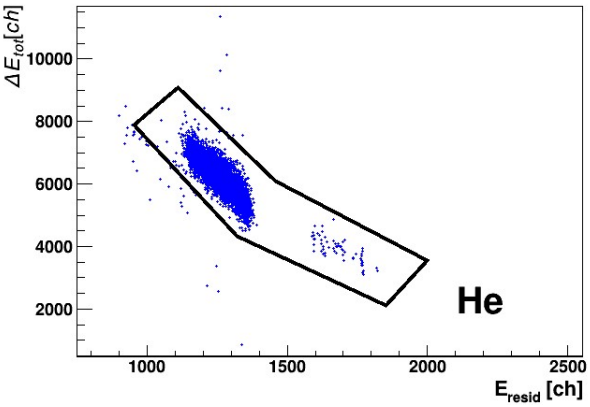

Fig. 1. A typical ΔE_{tot} versus residual energy (E_{resid}) spectrum for a single silicon detector of the FPD.

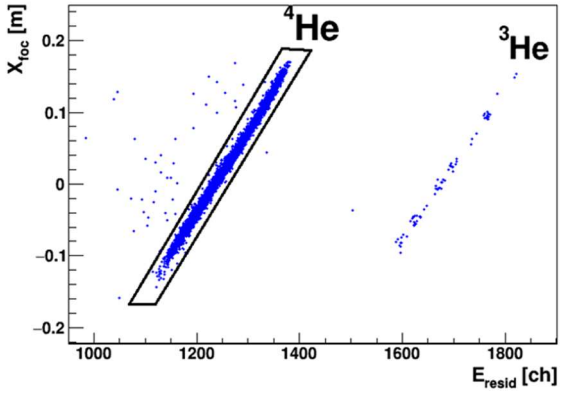

Fig. 2. Horizontal position (X_{foc}) versus residual energy (E_{resid}) spectrum for a single silicon detector of the FPD after applying the graphical selection on $Z = 2$ highlighted in Fig.1. The selection condition of ^{4}He events is illustrated by the solid black line.

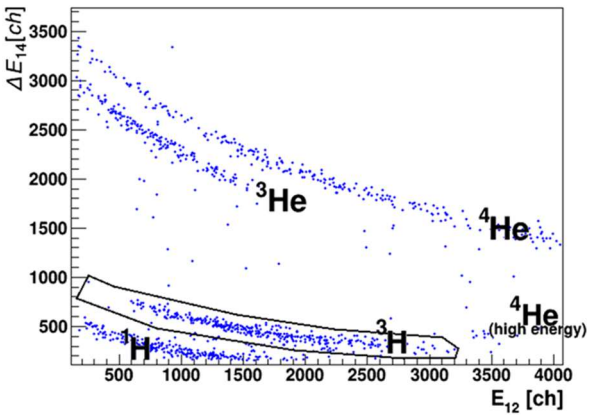

Fig. 3. A typical $\Delta E - E$ spectrum for a ΔE strip correlated with a single E pad of the OSCAR telescope. One can see the loci of protons, tritons, ^{3}He and ^{4}He while, the selection of tritons is depicted with the solid black line.

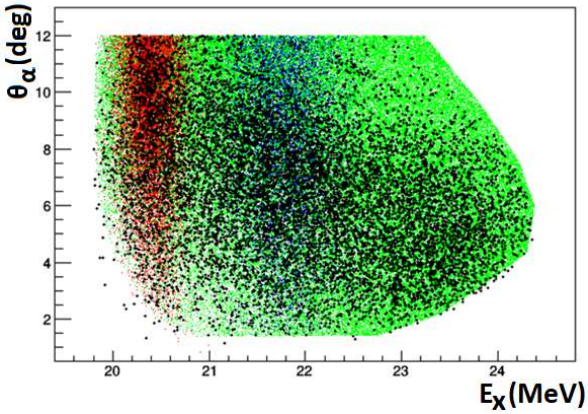

Fig. 4. A θ_α versus excitation energy (E_x) spectrum for the ^{4}He + ^{4}He → ^{4}He + ^{3}H + ^{1}H mode. The experimental data points, presented in black, were acquired in a ^{4}He - ^{3}H coincidence measurement. Preliminary simulations for the resonant (0^{+}) and the non-resonant continuum are presented with the red and green points, respectively, while the simulated events for the transfer are presented with the blue points. See text for more details.

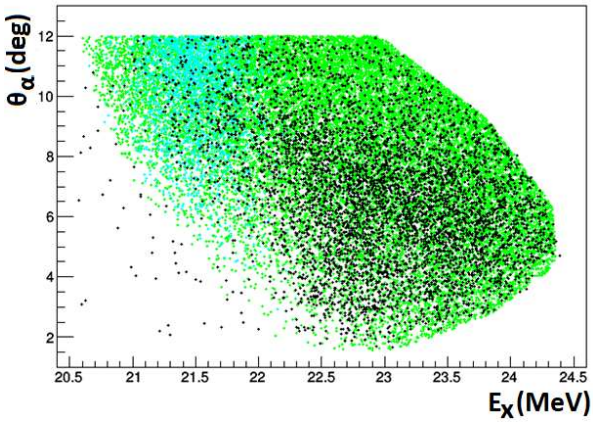

Fig. 5. A θ_α versus excitation energy (E_x) spectrum for the ^{4}He + ^{4}He → ^{4}He + ^{3}He + n mode. The experimental data points, presented in black, were acquired in a ^{4}He - ^{3}He coincidence measurement. Preliminary simulations for the non-resonant breakup and transfer are presented with the green and cyan blue points, respectively. See text for more details.

4 Summary

The $^4He + ^4He \rightarrow ^4He + ^3H + ^1H$ and $^4He + ^4He \rightarrow ^4He + ^3He + n$ reactions were measured at the MAGNEX facility of INFN – LNS together with the elastic scattering measurement. The challenging inelastic scattering measurement was performed in a coincidence measurement by detecting the heavy ejectile ^4He in MAGNEX while the lighter ^3H and ^3He were detected by the OSCAR telescope. The high Z and mass resolutions of both MAGNEX and OSCAR guaranteed an accurate particle identification. Comprehensive kinematical simulations based on the MULTIP algorithm make it feasible to disentangle between the inelastic scattering via the first excited state of ^4He (0^+), the non-resonant breakup processes and the transfer processes leading to the same final channels. The data analysis is underway in a more quantitative basis aiming to extract differential and integrated cross sections. A theoretical analysis is also in progress.

References

1. R. Frosch, R. E. Rand, M. R. Yearian et al., Phys. Lett. **19**, 155 (1965).
2. R. F. Frosch, R. E. Rand, H. Crannell et al., Nucl. Phys. A **110**, 657 (1968)
3. Th. Walcher, Phys. Lett. **B31**, 442 (1970).
4. G. Kobshall, C. Ottermann, K. Maurer et al., Nucl. Phys. A **405**, 648 (1983).
5. E. E. Gross, E. V. Hungerford III, J. J. Malanify et al., Phys. Rev. **178**, 1584 (1969).
6. M. Baumgartner, H. P. Gubler, M. Heller et al., Nucl. Phys. A **368**, 189 (1981).
7. S. Bacca, N. Barnea, W. Leidemann, G. Orlandini, Phys. Rev. Lett. **110**, 042503 (2013).
8. Y. Kucuk, M. Karakoç, A. Vitturi, Eur. Phys. J. A **57**, 37 (2021).
9. F. Cappuzzello, C. Agodi, D. Carbone, M. Cavallaro, Eur. Phys. J. A **52**, 167 (2016).
10. M. Cavallaro, F. Cappuzzello, D. Carbone, A. Cunsolo et al., Eur. Phys. J. A **48**, 59 (2012).
11. D. Torresi, O. Sgouros, V. Soukeras et al., Nucl. Instrum. Meth. Phys. Res. A **989**, 164918 (2021).
12. D. R. Tilley, H. R. Weller, G. M. Hale, Nucl. Phys. A **541**, 1 (1992).
13. D. Dell´Aquila, I. Lombardo, G. Verde et al., Nucl. Instrum. Meth. Phys. Res. A **877**, 227 (2018).
14. F. Cappuzzello, M. Cavallaro, A. Cunsolo, A. Foti et al., Nucl. Instrum. Meth. Phys. Res. A **621**, 419 (2010).
15. F. Cappuzzello, D. Carbone, M. Cavallaro, Nucl. Instrum. Meth. Phys. Res. A **638**, 74 (2011).
16. O. Sgouros, V. Soukeras, A. Pakou, Eur. Phys. J. A **53**, 165 (2017).
17. O. Sgouros, A. Pakou, D. Pierroutsakou et al., Phys. Rev. C **94**, 044623 (2016).
18. A. Pakou, O. Sgouros, V. Soukeras et al., Phys. Rev. C **95**, 044615 (2017).
19. V. Soukeras, A. Pakou, F. Cappuzzello et al., Phys. Rev. C **95**, 054614 (2017).
20. A. Pakou, O. Sgouros, V. Soukeras et al., Phys. Rev. C **101**, 024602 (2020).
21. A. Pakou, L. Acosta, P. D. O´Malley et al., Phys. Rev. C **102**, 031601(R) (2020).
22. V. Soukeras, O. Sgouros, A. Pakou et al., Phys. Rev. C **102**, 064622 (2020).
23. A. Pakou, O. Sgouros, V. Soukeras, F. Cappuzzello, Eur. Phys. J. A **57**, 25 (2021).
24. A. Pakou, O. Sgouros, V. Soukeras et al., Nucl. Phys. A **1008**, 122155 (2021).